Year: 2019

Preclinical Evaluation of Benzazepine-Based PET Radioligands (R)- and (S)-11C-Me-NB1 Reveals Distinct Enantiomeric Binding Patterns and a Tightrope Walk Between GluN2B- and 1-Receptor–Targeted PET Imaging

Haider, Ahmed ; Herde, Adrienne Müller ; Krämer, Stefanie D ; Varisco, Jasmine ; Keller, Claudia ; Frauenknecht, Katrin ; Auberson, Yves P ; Temme, Louisa ; Robaa, Dina ; Sippl, Wolfgang ; Schibli, Roger ; Wünsch, Bernhard ; Mu, Linjing ; Ametamey, Simon M

Abstract: The study aims to investigate the performance characteristics of the enantiomers of 11C-Me-NB1, a recently reported PET imaging probe that targets the GluN2B subunit of N-methyl-d-aspartate (NMDA) receptors. Methods: Reference compound Me-NB1 (inhibition constant for hGluN1/GluN2B, 5.4 nM) and the phenolic precursor were prepared via multistep synthesis. Following chiral resolution by high-performance liquid chromatography, enantiopure precursor compounds, (R)-NB1 and (S)-NB1, were labeled with 11C and validated in rodents using in vitro/ex vivo autoradiography, PET experiments, and dose-response studies. To illustrate the translational relevance, (R)- 11C-Me-NB1 was validated in autoradiographic studies using postmortem human GluN2B-rich cortical and GluN2B-deficient cerebellar brain slices. To determine target engagement, receptor occupancy was assessed at different plasma concentrations of CP101,606, a GluN2B receptor antagonist. Results: The radiosynthesis of (R)- and (S)- 11C-Me-NB1 was accomplished in 42% ± 9% (decay-corrected) radiochemical yields. Molar activity ranged from 40 to 336 GBq/ mol, and an excellent radiochemical purity of greater than 99% was achieved. Although (R)- 11C-Me-NB1 displayed heterogeneous accumulation with high selectivity for the GluN2B-rich forebrain, (S)- 11C-Me-NB1 revealed a homogeneous distribution across all brain regions in rodent brain autoradiograms and predominantly exhibited 1-receptor binding. Similar to rodent brain, (R)- 11C-Me-NB1 showed in postmortem human brain tissues higher binding in the cortex than in the cerebellum. Coincubation of the GluN2B-antagonist CERC-301 (1 M) reduced cortical but not cerebellar binding, demonstrating the specificity of (R)- 11C-Me-NB1 binding to the human GluN2B-containing NMDA receptor. In vivo specificity of (R)- 11C-Me-NB1 in the GluN2B-expressing cortex, striatum, thalamus, and hippocampus was demonstrated by PET imaging in rodents. Applying GluN2B-antagonist eliprodil, an evident dose-response behavior was observed with (R)- 11C-Me-NB1 but not with (S)- 11C-Me-NB1. Our findings further underline the tightrope walk between GluN2B- and 1-receptor-targeted imaging, illustrated by the entirely different receptor binding behavior of the 2 radioligand enantiomers. Conclusion: (R)- 11C-Me-NB1 is a highly selective and specific PET radioligand for imaging the GluN2B subunit of the NMDA receptor. The entirely different receptor binding behavior of (R)- 11C-Me-NB1 and (S)- 11C-Me-NB1 raises awareness of a delicate balance that is underlying the selective targeting of either GluN2B-carrying NMDA or 1-receptors.

DOI: https://doi.org/10.2967/jnumed.118.221051

Accepted Version

Originally published at:
Haider, Ahmed; Herde, Adrienne Müller; Krämer, Stefanie D; Varisco, Jasmine; Keller, Claudia; Frauenknecht, Katrin; Auberson, Yves P; Temme, Louisa; Robaa, Dina; Sippl, Wolfgang; Schibli, Roger; Wünsch, Bernhard; Mu, Linjing; Ametamey, Simon M (2019). Preclinical Evaluation of Benzazepine-Based PET Radioligands (R)- and (S)-11C-Me-NB1 Reveals Distinct Enantiomeric Binding Patterns and a Tightrope Walk Between GluN2B- and 1-Receptor–Targeted PET Imaging. Journal of Nuclear Medicine, 60(8):1167-1173.
DOI: https://doi.org/10.2967/jnumed.118.221051

Journal of Nuclear Medicine, published on January 25, 2019 as doi:10.2967/jnumed.118.221051

Preclinical Evaluation of Benzazepine-Based PET Radioligands *(R)*- and *(S)*-^{11}C-Me-NB1 Reveals Distinct Enantiomeric Binding Patterns and Tightrope Walk between GluN2B- and Sigma1 Receptor-Targeted PET Imaging

*Ahmed Haider[1], Adrienne Müller Herde[1], Stefanie D. Krämer[1], Jasmine Varisco[1], Claudia Keller[1], Katrin Frauenknech[2], Yves P. Auberson[3], Louisa Temme[4], Dina Robaa[5], Wolfgang Sippl[5], Roger Schibli[1,6], Bernhard Wünsch[4], Linjing Mu[1,6], Simon M. Ametamey[1]**

[1]Institute of Pharmaceutical Sciences, ETH Zurich, Vladimir-Prelog-Weg 4, CH-8093 Zurich, Switzerland

[2]Institute of Neuropathology, University of Zurich/University Hospital Zurich, CH-8091 Zurich, Switzerland

[3]Novartis Institutes for BioMedical Research, CH-4057 Basel, Switzerland

[4]Institute of Pharmaceutical and Medicinal Chemistry, University of Münster, D-48149 Münster, Germany

[5]Institute of Pharmacy, Martin-Luther University of Halle-Wittenberg, 06120 Halle/Saale, Germany

[6]Department of Nuclear Medicine, University Hospital Zurich, CH-8091 Zurich, Switzerland

Corresponding author:

Prof. Simon M. Ametamey

Radiopharmaceutical Sciences

Institute of Pharmaceutical Sciences

ETH Zurich

Vladimir-Prelog Weg 4

CH-8093 Zurich

Phone: +41 44 6337463

Fax: +41 44 6331367

Simon.Ametamey@pharma.ethz.ch

First author:

Ahmed Haider

Postdoctoral Researcher

Radiopharmaceutical Sciences

Institute of Pharmaceutical Sciences

ETH Zurich

Vladimir-Prelog Weg 4

CH-8093 Zurich

Phone: +41 44 6337364

Ahmed.Haider@pharma.ethz.ch

Word count: 4999

Short running title: Tightrope walk between GluN2B- and σ_1R-imaging

This project was supported by the Swiss National Science Foundation Grant Nr. 310030E-160403/1, the Clinical Research Priority Program on Multiple Sclerosis (CRPPMS) of the University of Zurich and the Stavros Niarchos Foundation.

ABSTRACT

The study aims to investigate the performance characteristics of the enantiomers of ^{11}C-Me-NB1, a recently reported positron emission tomography (PET) imaging probe that targets the GluN2B subtype of NMDA receptors. **Methods**: Reference compound Me-NB1 (K_i hGluN1/GluN2B = 5.4 nM) and the phenolic precursor were prepared via multistep synthesis. Upon chiral high-performance liquid chromatography resolution, enantiopure precursor compounds, *(R)*-NB1 and *(S)*-NB1, were labeled with carbon-11 and validated in rodents using *in vitro/ex vivo* autoradiography, PET experiments and dose-response studies. To illustrate the translational relevance, *(R)*-^{11}C-Me-NB1 was validated in autoradiographic studies using post-mortem human GluN2B-rich cortical and GluN2B-deficient cerebellar brain slices. To determine target engagement, receptor occupancy was assessed at different plasma concentrations of CP101,606, a GluN2B receptor antagonist. **Results**: The radiosynthesis of *(R)*- and *(S)*-^{11}C-Me-NB1 was accomplished in 42 ± 9 % (decay-corrected) radiochemical yields. Molar activity ranged from 40 – 336 GBq/µmol and an excellent radiochemical purity greater than 99% was achieved. While *(R)*-^{11}C-Me-NB1 displayed heterogeneous accumulation with high selectivity for the GluN2B-rich forebrain, *(S)*-^{11}C-Me-NB1 revealed a homogenous distribution across all brain regions in rodent brain autoradiograms, and predominantly exhibited σ1 receptor binding. Similar to rodent brain, *(R)*-^{11}C-Me-NB1 showed in post-mortem brain tissues higher binding in the cortex compared to the cerebellum. Co-incubation of the GluN2B-antagonist CERC-301 (1 µM) reduced cortical but not cerebellar binding, demonstrating the specificity of *(R)*-^{11}C-Me-NB1 binding to the human GluN2B-containing NMDA receptor. *In vivo* specificity of *(R)*-^{11}C-Me-NB1 in the GluN2B-expressing cortex, striatum, thalamus and hippocampus was demonstrated by PET imaging in rodents. Applying GluN2B-antagonist eliprodil, an evident dose-response behaviour was observed with *(R)*-^{11}C-Me-NB1 but not with *(S)*-^{11}C-Me-NB1. Our findings further underline the tightrope walk between GluN2B- and σ1 receptor-targeted imaging, illustrated by the entirely different receptor binding behavior of the two radioligand enantiomers. **Conclusion**: *(R)*-^{11}C-Me-NB1 is a highly selective and specific PET radioligand for imaging the GluN2B subunit of the *N*-methyl-D-aspartate (NMDA) receptor. The entirely different receptor binding behavior of *(R)*-^{11}C-Me-NB1 and *(S)*-^{11}C-Me-NB1 raises awareness of a delicate balance that is underlying the selective targeting of either GluN2B-carrying NMDA or σ_1 receptors.

Key words: PET imaging, GluN2B, σ_1-Receptor, Receptor occupancy, Neurodegeneration

INTRODUCTION

N-methyl-D-aspartate (NMDA) receptors are heterotetrameric assemblies of three distinct subunits GluN1, GluN2A-D as well as GluN3A/B and regulate numerous vital processes including neuronal development, synaptic plasticity, learning and memory functions in the mammalian central nervous system (CNS) (*1*). Upon engagement by the most abundant excitatory neurotransmitter L-glutamate and a co-agonist (glycine or D-serine), the ligand-gated ion channel undergoes a conformational change leading to the influx of sodium and calcium ions into the intracellular space (*2*). Owing to its high calcium ion permeability, over-activation of the NMDA receptor by excessive glutamatergic stimulation is associated with elevated intracellular calcium levels, ultimately leading to neuronal apoptosis (*3*). This insulting excitotoxic state has been described as one of the leading causes in the pathogenesis of various neurodegenerative and psychiatric disorders (*4*). Initial attempts to target the NMDA receptor resulted in the development of antagonists that act as channel blockers (*5*). Despite remarkable anti-excitotoxic properties, this class of compounds largely failed in clinical trials due to adverse psychotomimetic events (*1,6*). The poor safety profile was attributed to the mechanism of action, as channel blockers virtually suppress all NMDA receptor activity and therefore inhibit physiological processes that would require NMDA receptor signalling (*4*). Identification of the GluN2B-subunit as key contributor to excitotoxicity-induced apoptosis as well as the discovery of the N-terminal domain (NTD) binding site located at the interface between GluN1 and GluN2B, triggered a wave of enthusiasm and provided the opportunity for the design of subunit-selective NMDA receptor antagonists (*4*). In particular, GluN2B-selective drug candidates preserve the activity of non-GluN2B containing NMDA receptors, thereby exhibiting a favourable safety profile (*7,8*). Despite initial reports on GluN2B antagonists with high affinity and selectivity over other GluN2 subunits, successful clinical translation proved to be challenging due to off-target activity towards non-glutamatergic receptors such as the σ_1 receptor (σ_1R), a unique ligand-regulated molecular chaperone residing in the endoplasmatic reticulum (*9,10*). Indeed, improved measures assisting the *in vivo* evaluation of target engagement are crucial to ensure drug efficacy and to guide successful antagonist development (*11*). Consequently, validation tools to assess compound selectivity as well as *in vivo* receptor occupancy of GluN2B drug candidates are urgently needed.

Molecular imaging by non-invasive technologies such as positron emission tomography (PET) provides the possibility to study target engagement preclinically as well as clinically (*12*). Despite nearly two decades of preclinical research, no useful PET ligands exist for imaging GluN2B. Imaging probes reported so far have been plagued with four major limitations, namely considerable off-target binding, metabolic instability, low brain uptake as well as brain uptake not consistent with reported GluN2B expression patterns (*13*). In the mature brain, GluN2B-subunits are predominantly found in forebrain regions such as the striatum, hippocampus, cortex and thalamus, while the cerebellum only exhibits poor receptor subunit density (*1*). We recently reported on *(rac)*-^{11}C-Me-NB1, a GluN2B-specific PET probe that exhibits high target affinity (K_i to human GluN1/GluN2B of 5.4 nM) and excellent pharmacokinetic properties (*14*). In the present study, we describe remarkable differences in the *in vitro* and *in vivo* properties of the *S*- and *R*-enantiomers of ^{11}C-Me-NB1, confirmed by distinct enantiomeric target engagement. An autoradiographic blocker screening assay exploiting the distinct properties of *(R)*-^{11}C-Me-NB1 and *(S)*-^{11}C-Me-NB1 was developed, allowing to account for off-target activity towards σ_1R. In sharp contrast to *(S)*-^{11}C-Me-NB1, *(R)*-^{11}C-Me-NB1 exhibited excellent GluN2B-imaging properties as evidenced by autoradiographic studies on rodent brain tissues and PET imaging in Wistar rats. To illustrate the translational relevance, *(R)*-^{11}C-Me-NB1 was validated in autoradiographic studies using post-mortem human GluN2B-rich cortical and GluN2B-deficient cerebellar brain slices.

MATERIALS AND METHODS

In vitro Autoradiography

Post-mortem human brain samples from healthy volunteers were provided with written consent of the donors by the University Hospital of Zurich, Switzerland. Wistar rat and CD1 mouse brains and human brain tissue was embedded in Tissue-Tek® (O.C.T.) and prepared as 10 µm thick sections on a cryostat (Cryo-Star HM 560 MV; Microm, Thermo Scientific, Wilmington, DE, USA). Slices were adsorbed on SuperFrost® Plus (Menzel, Braunschweig, Germany) and stored at -80 °C until further use. For the autoradiography, slices were thawed on ice (15 min) and preconditioned for 10 min in an aqueous buffer containing (30 mM HEPES, 0.56 mM $MgCl_2$, 110 mM NaCl, 5 mM KCl, 3.3 mM $CaCl_2$ and 0.1 % fatty acid free bovine serum albumin (pH 7.4, 0 °C). The tissue samples were air-dried for 3 min at ambient temperature and subsequently incubated with either *(R)*- or *(S)*-^{11}C-Me-NB1 (3 nM, calculated based on the molar activity) for 20 minutes at 21 °C in a humidified chamber (complete tissue coverage with 1-2 mL per tissue slice required). For the blocker screening, 1 µM of either CERC-301, EVT-101, CP101,606, SA4503, fluspidine or *(+)*-pentazocine was applied. Upon completion of the incubation time, slices were decanted and washed 5 min in an aqueous buffer containing 30 mM HEPES, 0.56 mM $MgCl_2$, 110 mM NaCl, 5 mM KCl, 3.3 mM $CaCl_2$ and 0.1 % fatty acid free bovine serum albumin (pH 7.4, 0 °C). The samples were further washed (2 x 3 min) in an aqueous buffer containing 30 mM HEPES, 0.56 mM $MgCl_2$, 110 mM NaCl, 5 mM KCl, 3.3 mM $CaCl_2$ (pH 7.4) and (2 x 5 sec) in distilled water. Finally, the slices were dried and exposed to a phosphor imager plate (Fuji, Dielsdorf, Switzerland) for 30 minutes. The films were scanned by a BAS5000 reader (Fuji) and the data analysed using AIDA 4.50.010 software (Raytest Isotopenmessgeräte GmbH, Straubenhardt, Germany).

In vivo PET, Dose-Response and Receptor Occupancy Studies

All animal studies were conducted in accordance with the ARRIVE guidelines, the local Animal Protection Law and with further approval of the cantonal veterinary office in Zurich, Switzerland.

Wistar rats were purchased from Charles River (Sulzfeld, Germany) and kept in a room with controlled temperature (21°C) under a 12-hour light/12-hour dark cycle, with ad libitum access to food and water. Animals were allowed to acclimatize for one week before the start of the experiments. Animals were anesthetized with isoflurane and scanned in a PET/CT scanner (Super Argus, Sedecal, Madrid, Spain) for 60 min upon tail-vein injection of either *(R)*- or *(S)*-^{11}C-Me-NB1 (28 – 37 MBq, 0.5 – 2.3 nmol/kg). PET scans were followed by CT for anatomical orientation. For dose-response and receptor occupancy studies, eliprodil (0.002, 0.006, 0.02 and 2 mg/kg) and CP101,606 (0.3, 1, 3 and 10 mg/kg) in an aqueous vehicle (pH 7.0) consisting of glucose (5 %), NaCl (0.45 %) and citric acid (1 mM) for eliprodil and saline for CP101,606, respectively, were injection shortly before tracer administration. For the CP101,606 scans the blocker was further infused during the 60 min PET scan with the protocol (0.4, 1.3, 4 and 13.3 mg/kg/h) as illustrated in Supplemental Fig. 8. For baseline scans, the vehicle was injected shortly before tracer administration and further infused in the control animals of the CP101,606 study. Data reconstruction was carried out in user-defined time frames with a voxel size of 0.3875 x 0.3875 x 0.775 mm^3 as previously described by our group (*14*). Time-activity curves (TACs) were calculated by PMOD v3.7 (PMOD Technologies, Zurich, Switzerland) with predefined regions of interest as previously reported (*14*). Results are presented as standardized uptake values (SUVs), indicating the decay-corrected radioactivity per cm^3 divided by the injected dose per gram body weight. Receptor occupancy was calculated using Equations 1 and 2 in the supplemental information.

Ex vivo Autoradiography and Subsequent *in vitro* Displacement

(R)-^{11}C-Me-NB1 (522 MBq, 20.3 nmol/kg) was injected into a male Wistar rat and the animal was sacrificed under isoflurane anaesthesia by decapitation at 15 min p.i. The brain was dissected, embedded in Tissue-

Tek® (O.C.T.) and subsequently prepared as 10 µm thick coronal sections on a cryostat (Cryo-Star HM 560 MV; Microm, Thermo Scientific, Wilmington, DE, USA). For the displacement screening, tissue sections were incubated with 1 µM of either CERC-301, EVT-101, CP101,606. Fluspidine, *(+)*-pentazocine, *(S)*-Me-NB1 or vehicle (aqueous buffer containing 30 mM HEPES, 0.56 mM $MgCl_2$, 110 mM NaCl, 5 mM KCl, 3.3 mM $CaCl_2$ and 0.1 % fatty acid free bovine serum albumin, pH 7.4). Untreated sections were included for acquisition and analysis. The sections were exposed to a phosphor imager plate (Fuji, Dielsdorf, Switzerland) for 60 minutes and the film was scanned by a BAS5000 reader (Fuji). Data analysis was carried out by AIDA 4.50.010 software (Raytest Isotopenmessgeräte GmbH, Straubenhardt, Germany).

Statistical Analysis

Statistical probability values were calculated based on an independent two-tailed Student's test assuming normal distribution of the dataset (n = 4).

RESULTS

The organic syntheses of the desmethyl phenolic precursor NB1, reference compound Me-NB1, chiral separation of *(rac)*-Me-NB1 and the phenolic precursor *(rac)*-NB1 as well as radiolabeling procedures are described in the Supplemental Figs. 1-3. Absolute configurations of *(R)- and (S)*-Me-NB1 were determined by X-ray crystallography (Fig. 1A), and circular dichroism (CD) spectroscopy was used to confirm the stereochemistry of precursors *(R)*- and *(S)*-NB1 (Supplemental Fig. 3). Experimental procedure describing the X-ray crystallography can be found in Supplemental Fig. 2. Carbon-11 labeling of the *R*- and *S*-enantiomers of Me-NB1 was accomplished using ^{11}C-iodomethane in 42 ± 9 % radiochemical yield (decay corrected) and molar activity of 204 ± 80 GBq/μmol (n = 66). The radiochemical purity was greater than 99%. Autoradiographic experiments revealed significant differences between the binding patterns of *(R)*-^{11}C-Me-NB1 and *(S)*-^{11}C-Me-NB1 on rat brain tissue sections as shown in Fig. 1B. While *(S)*-^{11}C-Me-NB1 displayed a homogenous distribution across the whole brain, *(R)*-^{11}C-Me-NB1 revealed a heterogeneous distribution pattern with high binding to GluN2B-rich regions such as the cortex, striatum, thalamus and hippocampus. The cerebellum, a region with a low density of the GluN2B receptor subunit, showed lowest *(R)*-^{11}C-Me-NB1 binding. Similar results were obtained with mouse brain sections (Supplemental Fig. 4). In order to assess specificity and off-target binding towards σ_1R of both radiolabeled enantiomers, further *in vitro* autoradiographic experiments using a series of clinically tested ligands were undertaken. While *(R)*-^{11}C-Me-NB1 competed with GluN2B antagonists CERC-301, EVT-101 and CP101,606, the binding of *(S)*-^{11}C-Me-NB1 was abolished upon the addition of σ_1R ligands SA4503, fluspidine and (+)-pentazocine (Fig. 2). In accordance with *in vitro* autoradiography findings, competitive binding assays revealed Ki values of 511 nM for *R*-Me-NB1 and 74 nM for *S*-Me-NB1 towards the σ_1 receptor. Additionally, molecular dynamics (MD) simulations of the most stable docking poses showed that the (*R*)-enantiomer exhibits a favoured binding mode to the NTD binding site (Supplemental Figs. 5 and 6). It is common knowledge that enantiomers can exhibit different binding properties, however, our findings remarkably emphasize the tightrope walk between GluN2B- and σ_1R-targeted imaging.

Spurred by the *in vitro* and docking results, both enantiomerically pure radioligands were investigated in PET studies using male Wistar rats and time-activity curves were generated. Brain uptake was generally higher for the GluN2B-specific *R*-form and displayed a slower washout compared to the *S*-form. Consistently, and as expected, *(rac)*-^{11}C-Me-NB1 exhibited a time-activity curve that reflected the average of the characteristics of the two enantiomers (Fig. 3). An efficient blockade was observed upon injection of GluN2B-antagonist eliprodil (2 mg/kg). To assess the utility of *(R)*-^{11}C-Me-NB1 and *(S)*-^{11}C-Me-NB1 for dose-dependent target engagement, we performed dose-response experiments applying stepwise dose escalation of eliprodil (0.002, 0.006, 0.02 and 2 mg/kg). Fig. 4A shows a concentration-dependent blockade of the *R*-enantiomer which is reflected in the gradual decrease of time-activity curves with increasing eliprodil doses. In contrast, the *S*-enantiomer did not show a dose-dependent blockade, suggesting that *(S)*-^{11}C-Me-NB1 is not suitable for studying GluN2B target engagement by PET imaging (Fig. 4B). *(S)*-^{11}C-Me-NB1 was therefore not considered for further animal studies. An *in vitro* screening assay with non-radioactive *(R)*-Me-NB1 revealed no significant binding of the ligand to a series of prominent biological targets including, but not limited to, the muscarinic M_2, dopamine D_1 and D_3, adrenergic α_{1A} and α_{2A}, histamine H_3, serotonin, $GABA_A$, μ-opioid, noradrenalin transporter, MAO-A, VMAT2, VEGFR2, AChE, COX-1 and COX-2, androgen and progesterone receptors. One of the major challenges in the development of GluN2B-targeted PET radioligands is the lack of *in vivo* selectivity for GluN2B-rich brain regions (*15*). To address this question for *(R)*-^{11}C-Me-NB1, we performed an *ex vivo* autoradiography on a male Wistar rat brain. Highest tracer accumulation was found in the GluN2B-expressing cortex, striatum, thalamus as well as hippocampus while the GluN2B-deficient cerebellum revealed the lowest tracer binding of all brain regions (Fig. 5). To date, CP101,606 is the only GluN2B-selective antagonist with well-documented clinical efficacy (*16*). Therapeutic doses applied in clinical trials aim to reach a target plasma concentration of 200 ng/mL (*16*). We used *(R)*-^{11}C-Me-NB1 to assess the preclinical dose-dependent receptor occupancy of CP101,606 in male Wistar rats by PET imaging. In order to maintain the plasma concentration of CP101,606 at steady-state during the scan, the GluN2B-antagonist was first injected as a bolus, followed by continuous infusion. Blood samples were harvested after the PET scans with the aim to determine the steady-state

plasma concentration of CP101,606 for each dose. CP101,606 plasma concentrations in combination with the time-activity curves (Fig. 6A) were used to calculate the receptor occupancy (Fig. 6B) at different CP101,606 plasma concentrations according to Equations 1 and 2 that are described in the supplemental information. A D_{50} value (CP101,606 plasma concentration required for 50 % receptor occupancy) of 158 nmol/L (52 ng/mL) was deduced. Respective PET images are presented in Fig. 6C. Based on these results, the therapeutic CP101,606 plasma concentration of 611 nmol/L (200 ng/mL) occupies 80 % of the GluN2B binding sites in our rat model. These results highlight the importance of high receptor occupancy for efficacy. We further conducted a receptor occupancy study with CP101,606 and *(R)*-^{11}C-Me-NB1 using only bolus injections without any further infusions with the aim to challenge the need for labour-intensive infusion-based experimental setup. The study revealed that receptor occupancy results at identical bolus doses with and without infusions are comparable (Supplemental Fig. 8). *In vivo* specificity and selectivity of radioligands are conventionally evaluated by the injection of non-radioactive, high-affinity blockers in several-fold excess, however, this approach is confounded by the metabolism and pharmacokinetics of the blockers. In the absence of an efficient blockade, it remains unclear whether the blocker reached the biological target. To exclude confounding factors such as blocker metabolism and pharmacokinetics, we performed an *ex vivo* autoradiography on rat brain slices, followed by co-incubation of the dissected brain slices with different GluN2B and σ_1R ligands. In this autoradiographic displacement assay, CERC-301, EVT-101, CP101,606, fluspidine, (+)-pentazocine, *(S)*-Me-NB1 were used as displacing agents. The binding of *(R)*-^{11}C-Me-NB1 was displaced with the GluN2B antagonists (Fig. 7A), underlining the suitability of *(R)*-^{11}C-Me-NB1 as a GluN2B imaging agent. Biodistribution experiments conducted at 5, 15, 30, 45 and 60 min post injection (n = 4) confirmed that radioligand accumulation in the cortex was significantly higher than in the cerebellum at every measured time point. At the last measurement, 60 min post injection, the uptake for each GluN2B-expressing brain region was significantly higher compared to the cerebellum. The ratios to the cerebellum were: cortex/cerebellum (1.27 ± 0.07, $p < 0.01$), striatum/cerebellum (1.20 ± 0.06, $p < 0.05$), hippocampus/cerebellum (1.35 ± 0.05, $p < 0.01$) and thalamus/cerebellum (1.34 ± 0.05, $p < 0.01$). Biodistribution data is summarized in Supplemental Tables 2

and 3. Surprisingly, considerable tracer uptake in the Wistar rat brain stem was observed, which was blocked by eliprodil and CP101,606. Whether this uptake is related to GluN2B receptor binding or potential interactions with other GluN2-subtypes remains to be investigated. In order to pave the way for clinical translation, *(R)*-^{11}C-Me-NB1 was tested on post-mortem human brain sections by comparing healthy cortical with cerebellar brain tissue. In accordance with results obtained from the rodent brain, *(R)*-^{11}C-Me-NB1 displayed higher binding in the cortex than in the cerebellum (Fig. 7B). Co-incubation of the GluN2B-antagonist CERC-301 (1 μM) reduced cortical but not cerebellar binding, thus, demonstrating the specificity of *(R)*-^{11}C-Me-NB1 binding to the human GluN2B-containing NMDA receptor.

DISCUSSION

The present study revealed a remarkable enantioselectivity of *(R)*-^{11}C-Me-NB1 over *(S)*-^{11}C-Me-NB1 for GluN2B-containing NMDA receptors as demonstrated by distinct autoradiographic binding patterns on rat and mouse brain sections, molecular dynamics studies and by *in vivo* dose-response experiments. Blocker screening assays with GluN2B- and σ_1R-selective ligands showed entirely different binding properties of the two radiolabeled enantiomers, thereby raising awareness of the tightrope walk between GluN2B- and σ_1R-targeted PET imaging. While *(R)*-^{11}C-Me-NB1 is a GluN2B-ligand, *(S)*-^{11}C-Me-NB1 binds predominantly to the σ_1 receptor. Although there is precedence for showing distinct pharmacological activities by two enantiomers of a given compound, which in part could be related differences in brain uptake kinetics (*17,18*), the extent to which *(R)*- and *(S)*-^{11}C-Me-NB1 reveal different preferences for GluN2B-subunits and σ_1 receptors in the brain is rather remarkable. To our knowledge, there is no PET radioligand reported in the literature that shows such distinct enantiomer-related characteristics for two pharmacogologically and closely related receptors. GluN2B-antagonists are generally well tolerated preclinically and clinically, however, representative drug candidates such as CERC-301 (MK-0657) failed to demonstrate efficacy in clinical trials (*19-22*). A phase II clinical trial of EVT-101 was terminated due to difficulties in patient recruitment (ClinicalTrials.gov identifier: NCT01128452). No data on the clinical efficacy has so far been disclosed. Although CERC-301 and EVT-101 competed with *(R)*-^{11}C-Me-NB1 during *in vitro* autoradiography, we did not observe any competition for doses up to 2 mg/kg in preliminary PET experiments with male Wistar rats (Supplemental Fig. 9). To understand the differences between *in vitro* and *in vivo* findings, we performed an *ex vivo* metabolite study and confirmed the presence of intact *(R)*-^{11}C-Me-NB1 and the absence of radiometabolites in Wistar rat brain. An *ex vivo* autoradiography with subsequent displacement of *(R)*-^{11}C-Me-NB1 by CERC-301 and EVT-101 further confirmed that the radiotracer remains intact and that both CERC-301 and EVT-101 bind to the same binding site. We therefore hypothesize that CERC-301 and EVT-101 exhibit unfavourable in vivo pharmacokinetic and/or metabolic properties in rodents, which led to the absence of target engagement *in vivo*. Confirmation of these findings

in a clinical setup would shed more light on why these orally available GluN2B-antagonists are not living up to their expectations with respect to clinical efficacy. In sharp contrast to CERC-301 and EVT-101, the GluN2B-antagonists CP101,606 and eliprodil efficiently blocked *(R)*-^{11}C-Me-NB1 in the rodent brain not only *in vitro* but also *in vivo*. Receptor occupancy studies revealed that the clinically applied target plasma concentration of CP101,606 occupies the majority of NTD binding sites, which is in accordance with the clinical efficacy reported upon patient treatment with CP101,606 (*16,21,23*). Finally, to demonstrate the translational relevance of our new radioligand, we performed autoradiographic studies using post-mortem human GluN2B-rich cortical and GluN2B-deficient cerebellar brain sections. The results further showed that *(R)*-^{11}C-Me-NB1 binds specifically, and is sensitive in detecting the GluN2B-subunits of the NMDA receptor in post-mortem human brain tissue samples. To the best of our knowledge, this is the first report on a GluN2B PET radioligand that exhibits a combination of specificity and selectivity *in vitro* as well as *in vivo* with appropriate pharmacokinetic properties, characterized by high brain uptake and no brain radiometabolites (Supplemental Fig. 7).

Successful clinical validation of *(R)*-^{11}C-Me-NB1 would enable the assessment of emerging GluN2B-antagonists by means of target engagement studies and ultimately lead to accurate patient dosing. Moreover, the availability of a selective GluN2B PET radioligand will allow to elucidate the role of GluN2B-carrying NMDA receptors in patients with neurodegenerative and psychiatric disorders.

CONCLUSION

After nearly two decades of preclinical research, we here report on a successful NMDA PET radioligand that exhibits a combination of GluN2B-specificity and selectivity *in vitro* and *in vivo*. *(R)*-^{11}C-Me-NB1 revealed outstanding tracer characteristics and outperformed *(S)*-^{11}C-Me-NB1. *(R)*-^{11}C-Me-NB1 has great potential for imaging numerous psychiatric and brain diseases in which the GluN2B subunit of the NMDA receptor is implicated. This new radioligand holds promise both preclinically and clinically for the selection of appropriate doses of candidate drugs that bind to the GluN2B subunit of the NMDA receptor.

Disclosure

This project was supported by the Swiss National Science Foundation Grant Nr. 310030E-160403/1, the Clinical Research Priority Program on Multiple Sclerosis (CRPPMS) of the University of Zurich and the Stavros Niarchos Foundation. The present work is related to a recently filed patent application (US20170224852A1).

ACKNOWLEDGEMENT

Mr. Bruno Mancosu is acknowledged for the technical support with the carbon-11 module. We thank Dr. Silvan Boss for the assistance with the chiral purification and Hui Yuan Oliver for the support during biodistribution studies and Dr. Tao Sun for the support with the precursor synthesis. The technical assistance of Mrs. Irina Abakumova and Magdalena Foege is kindly acknowledged. We thank Dr. Ina Dix for the X-ray crystallography and acknowledge Prof. Roland Martin for organizing tissue samples.

REFERENCES

1. Paoletti P, Bellone C, Zhou Q. NMDA receptor subunit diversity: impact on receptor properties, synaptic plasticity and disease. *Nat Rev Neurosci.* 2013;14:383-400.

2. Traynelis SF, Wollmuth LP, McBain CJ, et al. Glutamate receptor ion channels: structure, regulation, and function. *Pharmacol Rev.* 2010;62:405-496.

3. Sattler R, Tymianski M. Molecular mechanisms of calcium-dependent excitotoxicity. *J Mol Med.* 2000;78:3-13.

4. Hardingham GE. Coupling of the NMDA receptor to neuroprotective and neurodestructive events. *Biochem Soc Trans.* 2009;37:1147-1160.

5. Anis NA, Berry SC, Burton NR, Lodge D. The dissociative anaesthetics, ketamine and phencyclidine, selectively reduce excitation of central mammalian neurones by N-methyl-aspartate. *Br J Pharmacol.* 1983;79:565-575.

6. Hardingham GE, Bading H. Synaptic versus extrasynaptic NMDA receptor signalling: implications for neurodegenerative disorders. *Nat Rev Neurosci.* 2010;11:682-696.

7. Mony L, Kew JN, Gunthorpe MJ, Paoletti P. Allosteric modulators of NR2B-containing NMDA receptors: molecular mechanisms and therapeutic potential. *Br J Pharmacol.* 2009;157:1301-1317.

8. Karakas E, Simorowski N, Furukawa H. Subunit arrangement and phenylethanolamine binding in GluN1/GluN2B NMDA receptors. *Nature.* 2011;475:249-253.

9. Contreras PC, Bremer ME, Gray NM. Ifenprodil and SL 82.0715 potently inhibit binding of [^{3}H](+)-3-PPP to sigma binding sites in rat brain. *Neurosci Lett.* 1990;116:190-193.

10. Maurice T, Su TP. The pharmacology of sigma-1 receptors. *Pharmacol Ther.* 2009;124:195-206.

11. Kemp JA, McKernan RM. NMDA receptor pathways as drug targets. *Nat Neurosci.* 2002;5 Suppl:1039-1042.

12. Slough C, Masters SC, Hurley RA, Taber KH. Clinical positron emission tomography (PET) neuroimaging: Advantages and limitations as a diagnostic tool. *J Neuropsychiatry Clin Neurosci.* 2016;28:A4, 67-71.

13. Fuchigami T, Nakayama M, Yoshida S. Development of PET and SPECT probes for glutamate receptors. *ScientificWorldJournal.* 2015;2015:716514.

14. Kramer SD, Betzel T, Mu L, et al. Evaluation of (11)C-Me-NB1 as a potential PET radioligand for measuring GluN2B-containing NMDA receptors, drug occupancy, and receptor cross talk. *J Nucl Med.* 2018;59:698-703.

15. Roger G, Dolle F, De Bruin B, et al. Radiosynthesis and pharmacological evaluation of [11C]EMD-95885: a high affinity ligand for NR2B-containing NMDA receptors. *Bioorg Med Chem.* 2004;12:3229-3237.

16. Nutt JG, Gunzler SA, Kirchhoff T, et al. Effects of a NR2B selective NMDA glutamate antagonist, CP-101,606, on dyskinesia and Parkinsonism. *Mov Disord.* 2008;23:1860-1866.

17. Brust P, Deuther-Conrad W, Becker G, et al. Distinctive in vivo kinetics of the new sigma1 receptor ligands (R)-(+)- and (S)-(-)-18F-fluspidine in porcine brain. *J Nucl Med.* 2014;55:1730-1736.

18. Kranz M, Sattler B, Tiepolt S, et al. Radiation dosimetry of the alpha4beta2 nicotinic receptor ligand (+)-[(18)F]flubatine, comparing preclinical PET/MRI and PET/CT to first-in-human PET/CT results. *EJNMMI Phys.* 2016;3:25.

19. Amico-Ruvio SA, Paganelli MA, Myers JM, Popescu GK. Ifenprodil effects on GluN2B-containing glutamate receptors. *Mol Pharmacol.* 2012;82:1074-1081.

20. Garner R, Gopalakrishnan S, McCauley JA, et al. Preclinical pharmacology and pharmacokinetics of CERC-301, a GluN2B-selective N-methyl-D-aspartate receptor antagonist. *Pharmacol Res Perspect.* 2015;3:198.

21. Preskorn SH, Baker B, Kolluri S, Menniti FS, Krams M, Landen JW. An innovative design to establish proof of concept of the antidepressant effects of the NR2B subunit selective N-methyl-D-aspartate antagonist, CP-101,606, in patients with treatment-refractory major depressive disorder. *J Clin Psychopharmacol.* 2008;28:631-637.

22. Ibrahim L, Diaz Granados N, Jolkovsky L, et al. A Randomized, placebo-controlled, crossover pilot trial of the oral selective NR2B antagonist MK-0657 in patients with treatment-resistant major depressive disorder. *J Clin Psychopharmacol.* 2012;32:551-557.

23. Bullock MR, Merchant RE, Carmack CA, et al. An open-label study of CP-101,606 in subjects with a severe traumatic head injury or spontaneous intracerebral hemorrhage. *Ann N Y Acad Sci.* 1999;890:51-58.

Figures

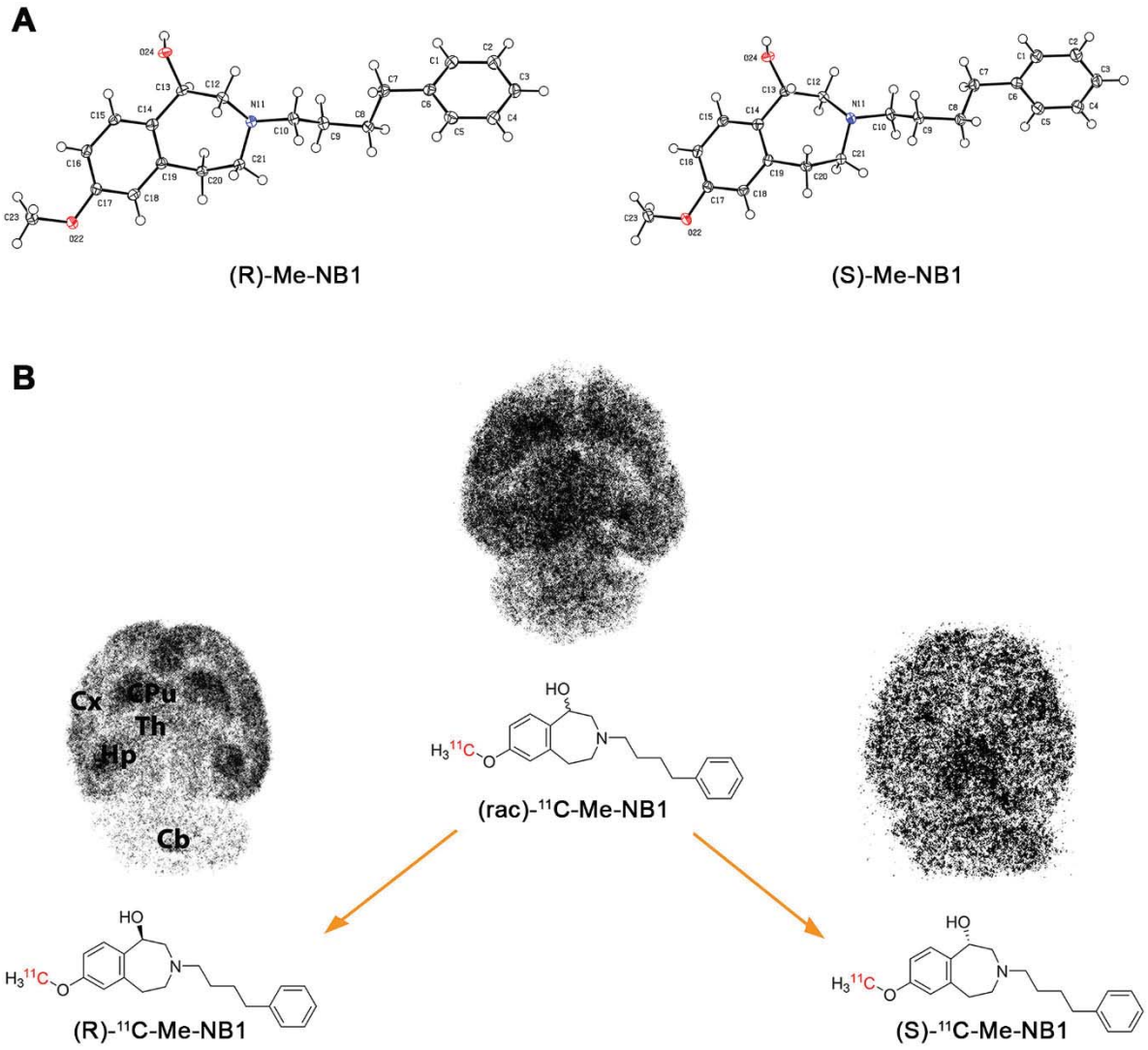

Figure 1: Absolute configuration and binding behaviour of *(R)*- and *(S)*-Me-NB1 **A.** ORTEP view of *(R)*- and *(S)*-Me-NB1 in the solid state. Me-NB1 exhibits one chiral centre depicted at position C13. Thermal ellipsoids are set to 30 % probability. For all non-hydrogen atoms, anisotropic displacement parameters were used. Hydrogen atoms were refined in idealized positions using a riding model. **B**. Representative in vitro autoradiograms of *(R)/(S)*-^{11}C-Me-NB1 incubated with Wistar rat brain sections. While the *S*-enantiomer binds to virtually all brain regions, the *R*-enantiomer exhibits selectivity for the GluN2B-rich forebrain. Cx: cortex, CPu: corpus striatum, Hp: hippocampus, Th: thalamus, Cb: cerebellum.

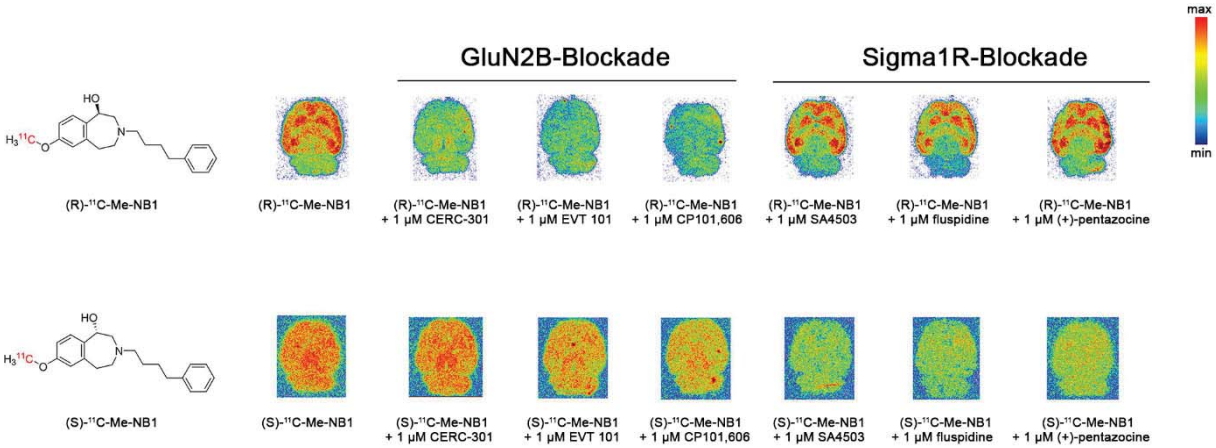

Figure 2: Autoradiographic screening of clinically tested GluN2B ligands CERC-301, EVT-101 and CP101,606 as well as σ_1R ligands SA4503, fluspidine and (+)-pentazocine as blocking agents for *(R)*-^{11}C-Me-NB1 and *(S)*-^{11}C-Me-NB1. *(R)*-^{11}C-Me-NB1 showed a heterogeneous binding behaviour which was GluN2B-specific while *(S)*-^{11}C-Me-NB1 exhibited considerable σ_1R binding.

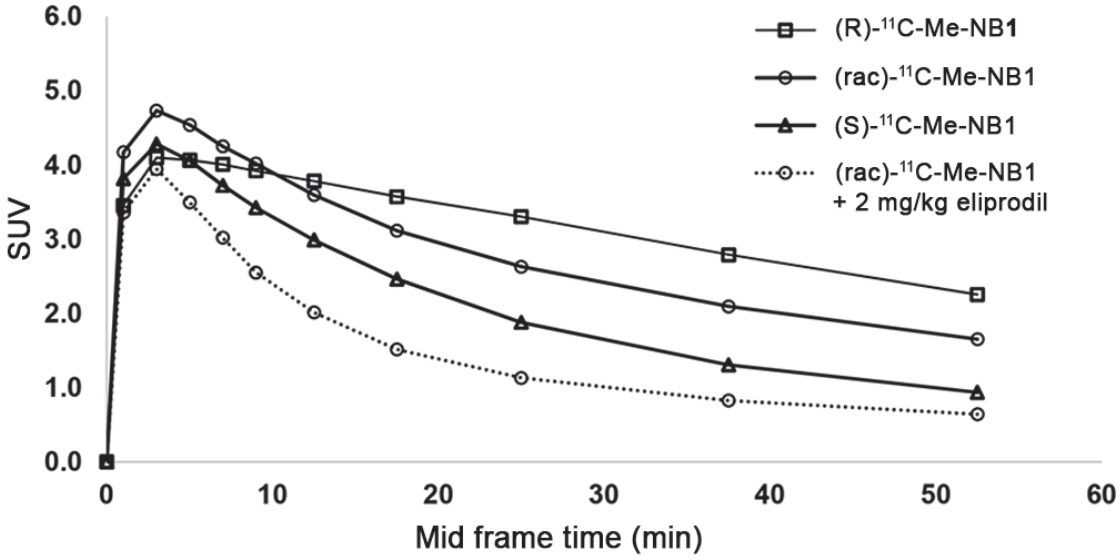

Figure 3: Whole-brain time-activity curves of racemic and enantiomerically pure ^{11}C-Me-NB1 in the Wistar rat brain are depicted as standardized uptake values (SUVs). The GluN2B-specific *R*-form exhibited higher SUVs than the S-form, while the racemic mixture displayed a time-activity curve that lies between both enantiomers. For the blockade experiment, 2 mg/kg of GluN2B antagonist eliprodil was used.

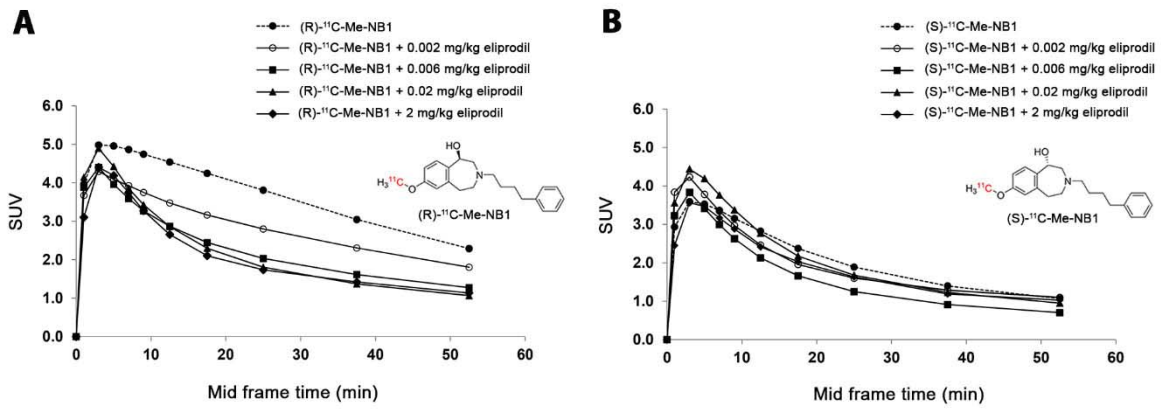

Figure 4: Dose-response curves of *(R)*-^{11}C-Me-NB1 and *(S)*-^{11}C-Me-NB1 with eliprodil in the Wistar rat brain. Results are reported as standardized uptake values (SUVs) calculated from PET experiments (0-60 min). **A**. *(R)*-^{11}C-Me-NB1 revealed a consistent dose-response profile upon stepwise dose escalation of eliprodil. **B**. *(S)*-^{11}C-Me-NB1 does not show a dose-dependent blockade.

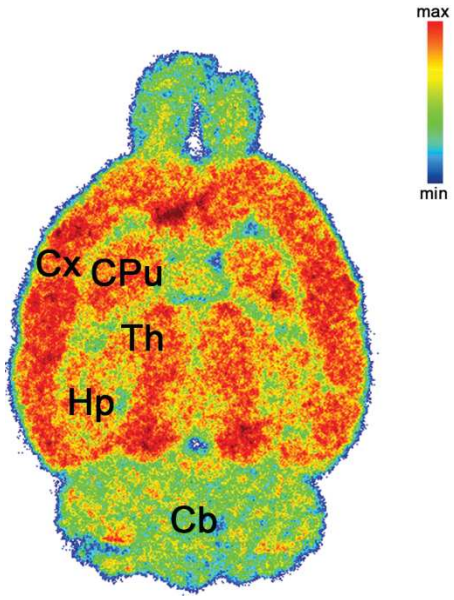

Figure 5: Representative *ex vivo* autoradiogram of a Wistar rat brain at 15 min post injection of *(R)*-^{11}C-Me-NB1. Selectivity for the cortex, striatum, thalamus and hippocampus over the cerebellum was observed. Cx: cortex, CPu: corpus striatum, Hp: hippocampus, Th: thalamus, Cb: cerebellum.

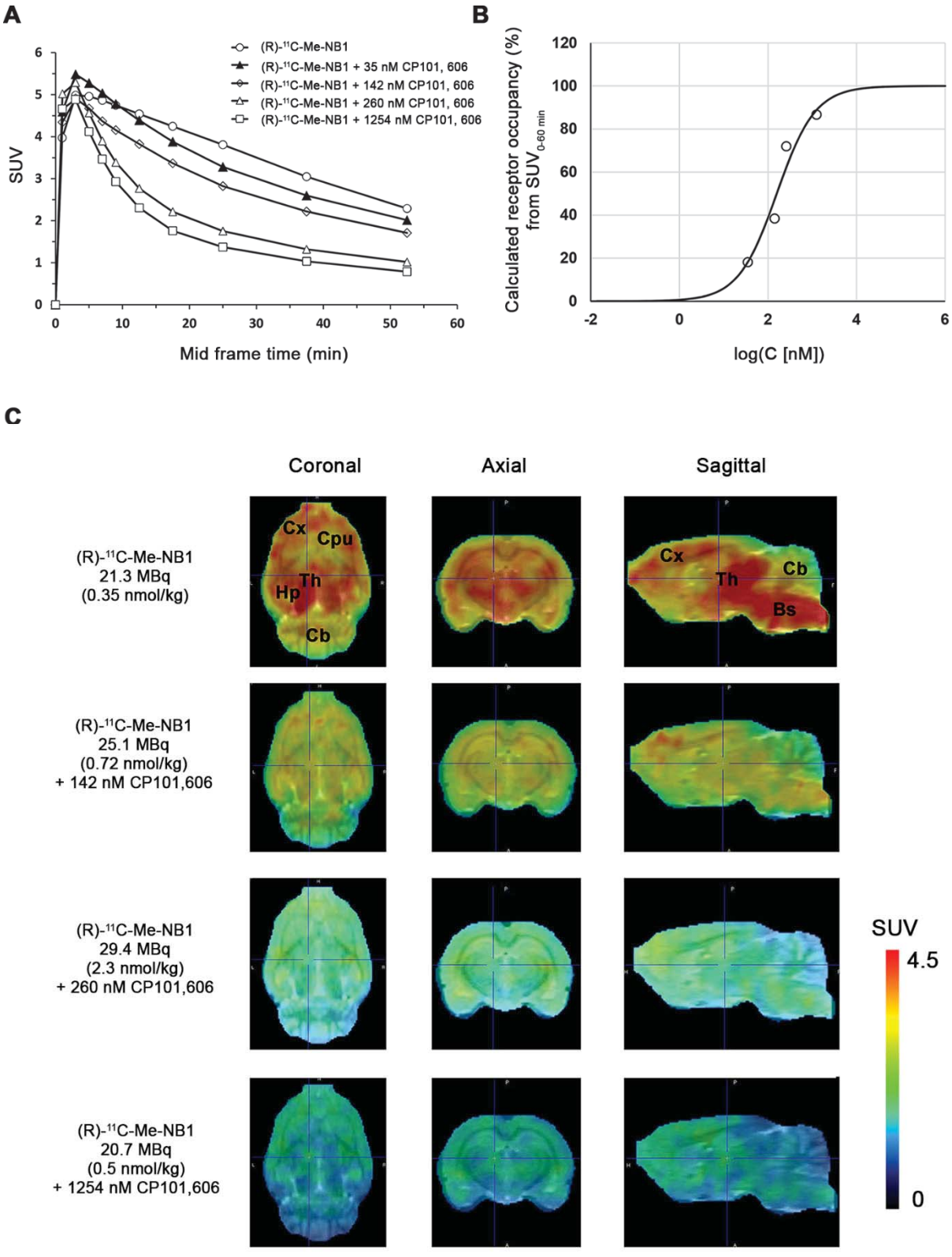

Figure 6: Receptor occupancy (RO) by the clinically tested GluN2B antagonist CP101,606 and *(R)*-^{11}C-Me-NB1 in Wistar rats (panel **B**), calculated from experimental $SUV_{0\text{-}60\ min}$ (panel **A**), revealed a D_{50} value of 158 nmol/L or 52 ng/mL (plasma

concentration required for 50 % receptor occupancy). The clinically applied target plasma concentration of 200 ng/mL occupies 80 % of the GluN2B binding sites in our rat model. Rat brain PET images were superimposed on a PMOD MRI template (panel **C**). Cx: cortex, CPu: corpus striatum, Hp: hippocampus, Th: thalamus, Cb: cerebellum, Bs: brain stem.

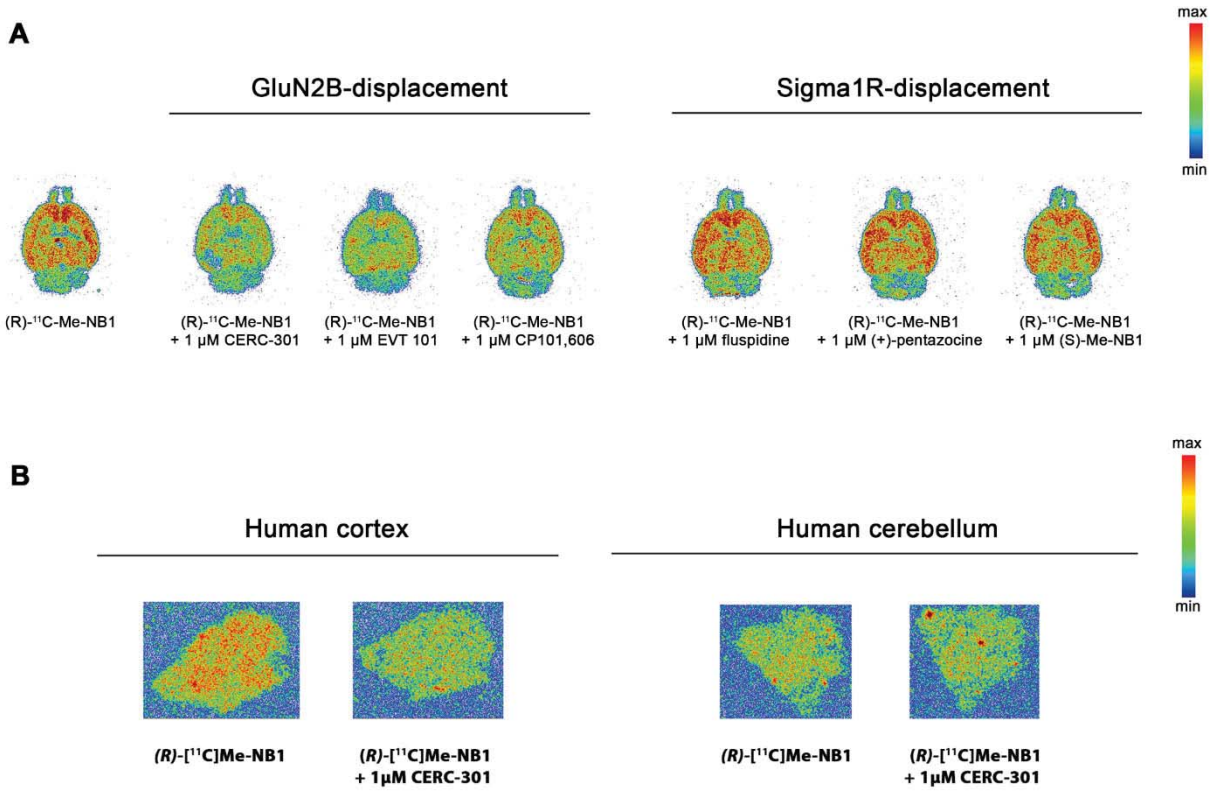

Figure 7: Representative autoradiograms on rodent and human brain tissue. **A.** *Ex vivo* autoradiography at 15 min post injection of *(R)*-^{11}C-Me-NB1 into a Wistar rat and subsequent *in vitro* displacer screening with GluN2B ligands CERC-301, EVT-101, CP101,606 and σ_1R ligands fluspidine, (+)-pentazocine as well as *(S)*-Me-NB1. Displacement of *(R)*-^{11}C-Me-NB1 binding is only observed for the GluN2B antagonists. **B**. Representative autoradiograms of *(R)*-^{11}C-Me-NB1 incubated with human post-mortem brain sections. GluN2B-specific binding was observed in the temporal cortex (indicated by the blockade experiment with GluN2B antagonist CERC-301), while the cerebellum did not reveal any specific binding of the radioligand.

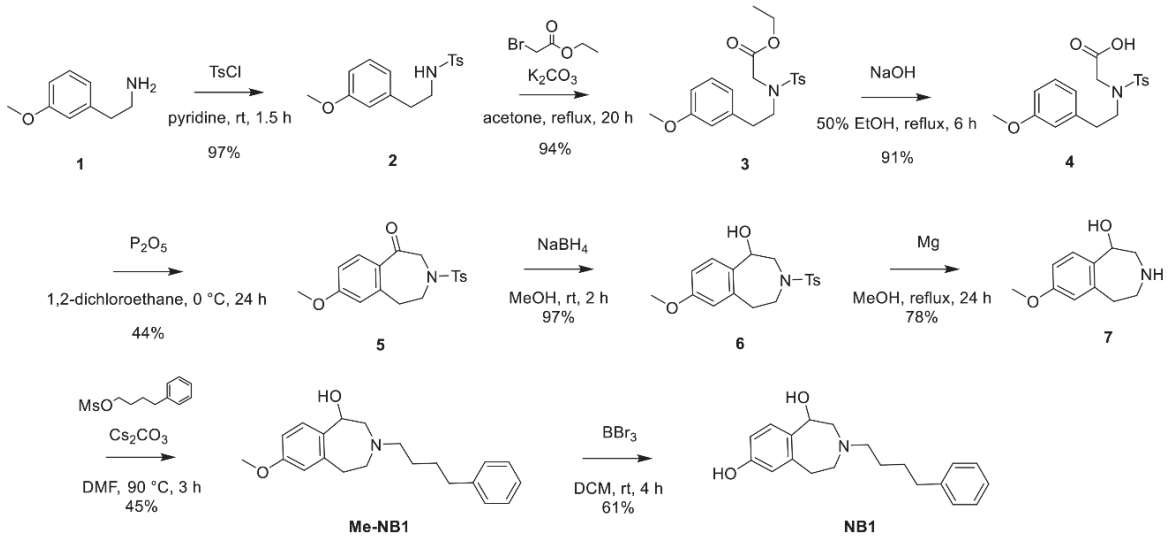

Supplemental Figure 1: Synthesis of reference compound **Me-NB1** and of the phenolic precursor **NB1** .

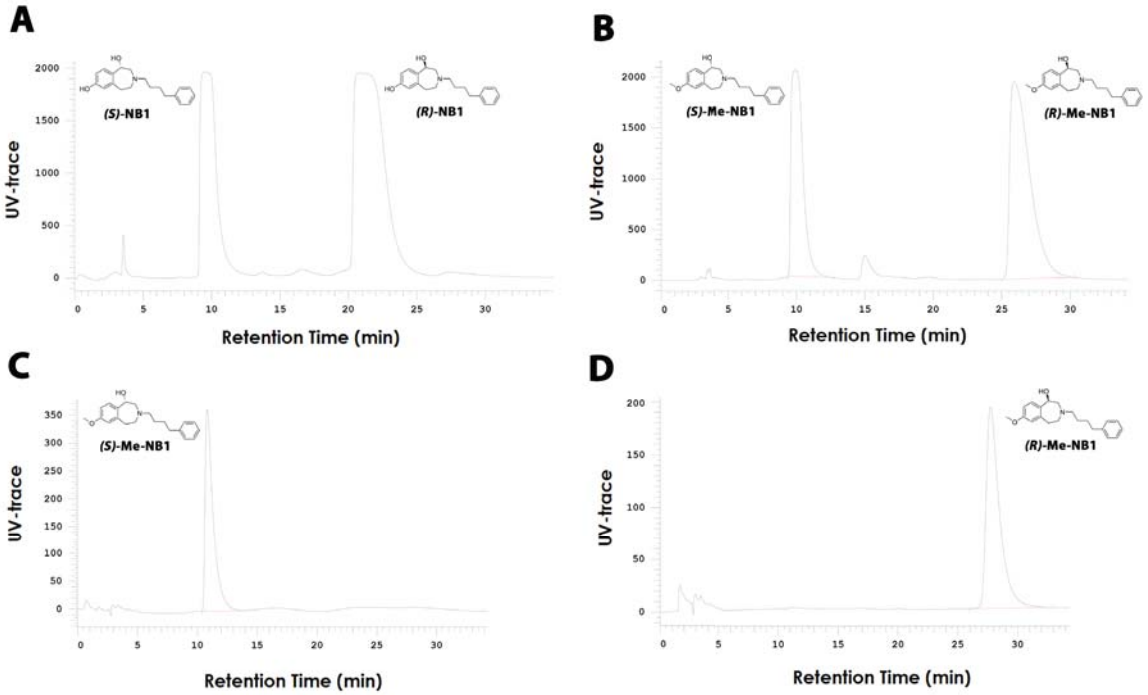

Supplemental Figure 2: Chiral HPLC separation of Me-NB1 and NB1 under isocratic normal phase conditions (hexane/isopropanol 8:2). **A.** Semipreparative chromatogram after chiral resolution of *(rac)*-NB1. **C.** Semipreparative chromatogram after chiral resolution of *(rac)*-Me-NB1. **C.** Quality control of *(S)*-Me-NB1 **D.** Quality control of *(R)*-Me-NB1.

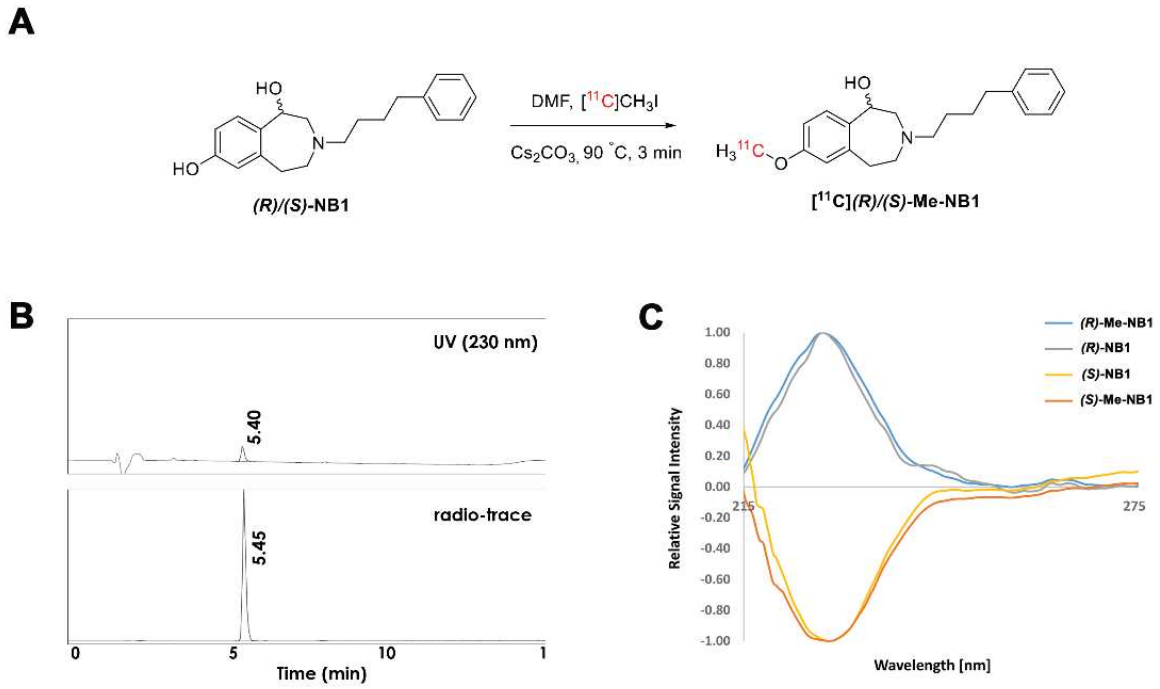

Supplemental Figure 3: A. Radiolabeling of ***(R)*- and *(S)*-^{11}C-Me-NB1** was achieved by treatment of the phenolic precursor in analogy to the procedure recently published by our group . **B.** Quality control of formulated tracer by UV- and radio-trace. **C**. Circular dichroism spectra recorded in the range between 215 – 275 nm for *(R)*-Me-NB1, *(S)*-Me-NB1, *(R)*-NB1 and *(S)*-NB1.

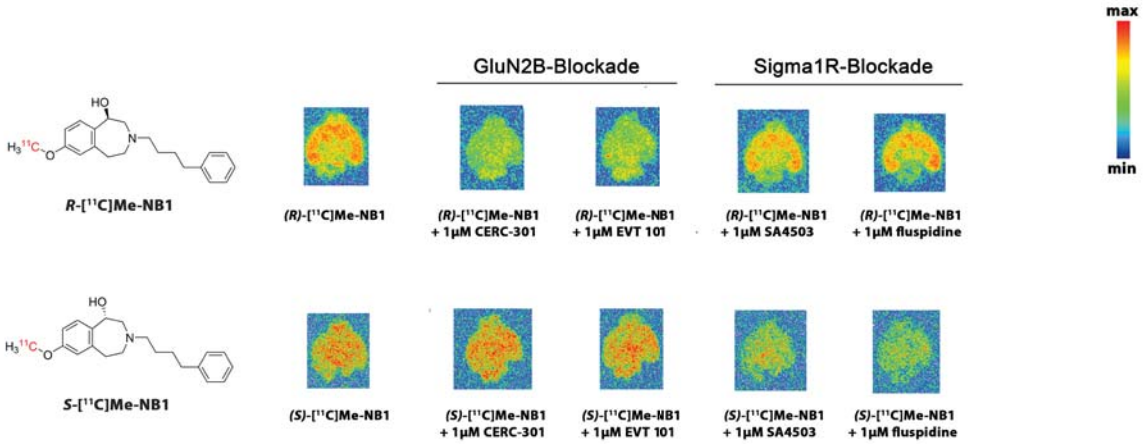

Supplemental Figure 4: Representative autoradiograms of *(R)*-^{11}C-Me-NB1 and *(S)*-^{11}C-Me-NB1 on coronal mouse brain sections. The binding of *(R)*-^{11}C-Me-NB1 was heterogeneous and GluN2B-specific while *(S)*-^{11}C-Me-NB1 showed considerable σ_1R binding. The blocking studies revealed selectivity of the *R*-enantiomer over σ_1R. In contrast, the *S*-enantiomer exhibited considerable binding to the σ_1 receptor.

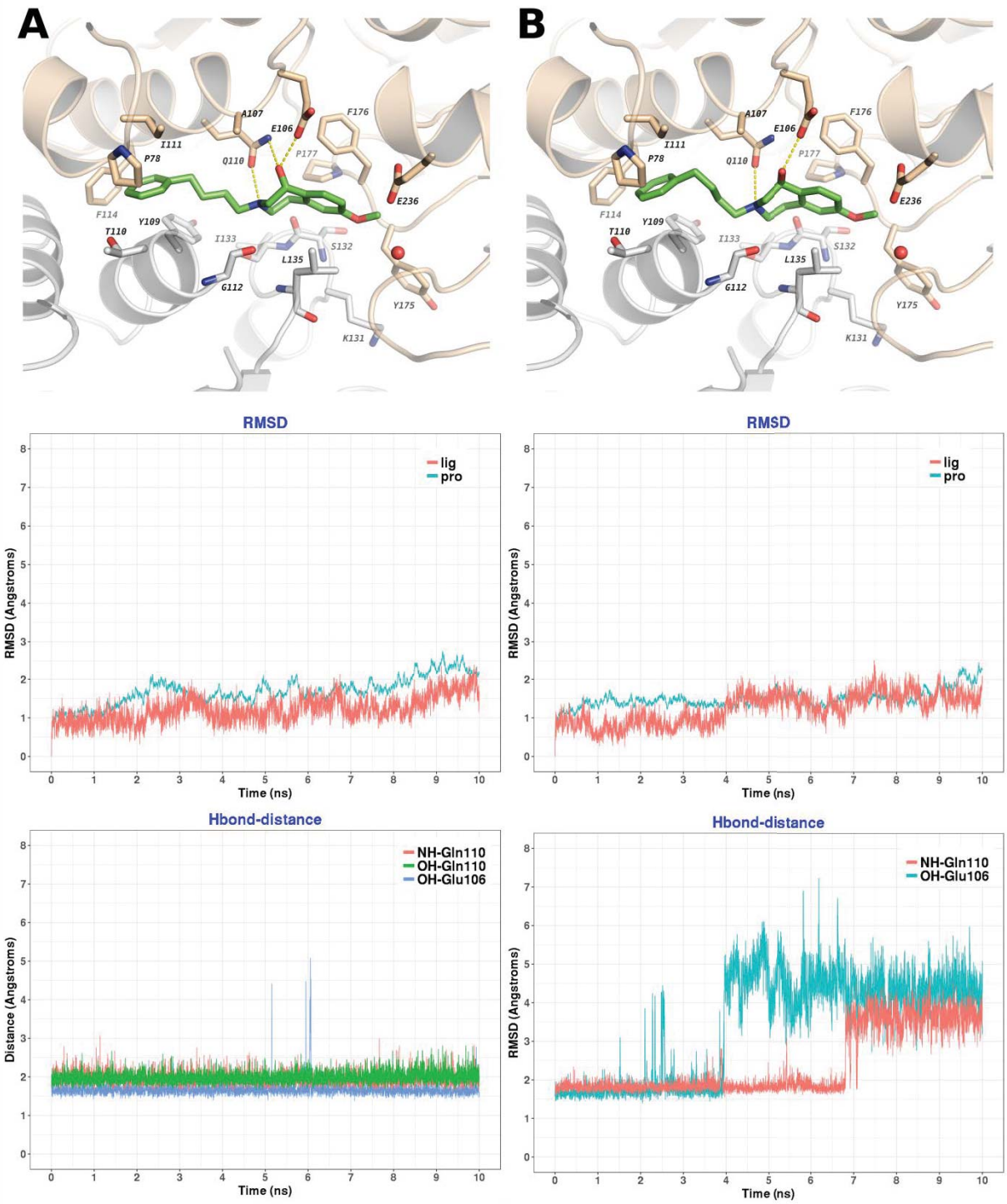

Supplemental Figure 5: Molecular dynamics simulation of the most stable *(R)*-Me-NB1 and *(S)*-Me-NB1 binding modes and stability of the predicted hydrogen-bond interactions. **A**. *(R)*-Me-NB1 interactions were observed between the ligand NH-group and glutamine 110 as well as the ligand OH-group and both glutamate 106 and glutamine 110 of the GluN2B subunit. Hydrogen bonds were maintained during MD. **B**. *(S)*-Me-NB1 interactions were observed between the ligand NH-group and glutamine 110

as well as the ligand OH-group and glutamate 106. No interaction between ligand OH-group and glutamine 110 was predicted. Hydrogen bonds were not maintained during MD.

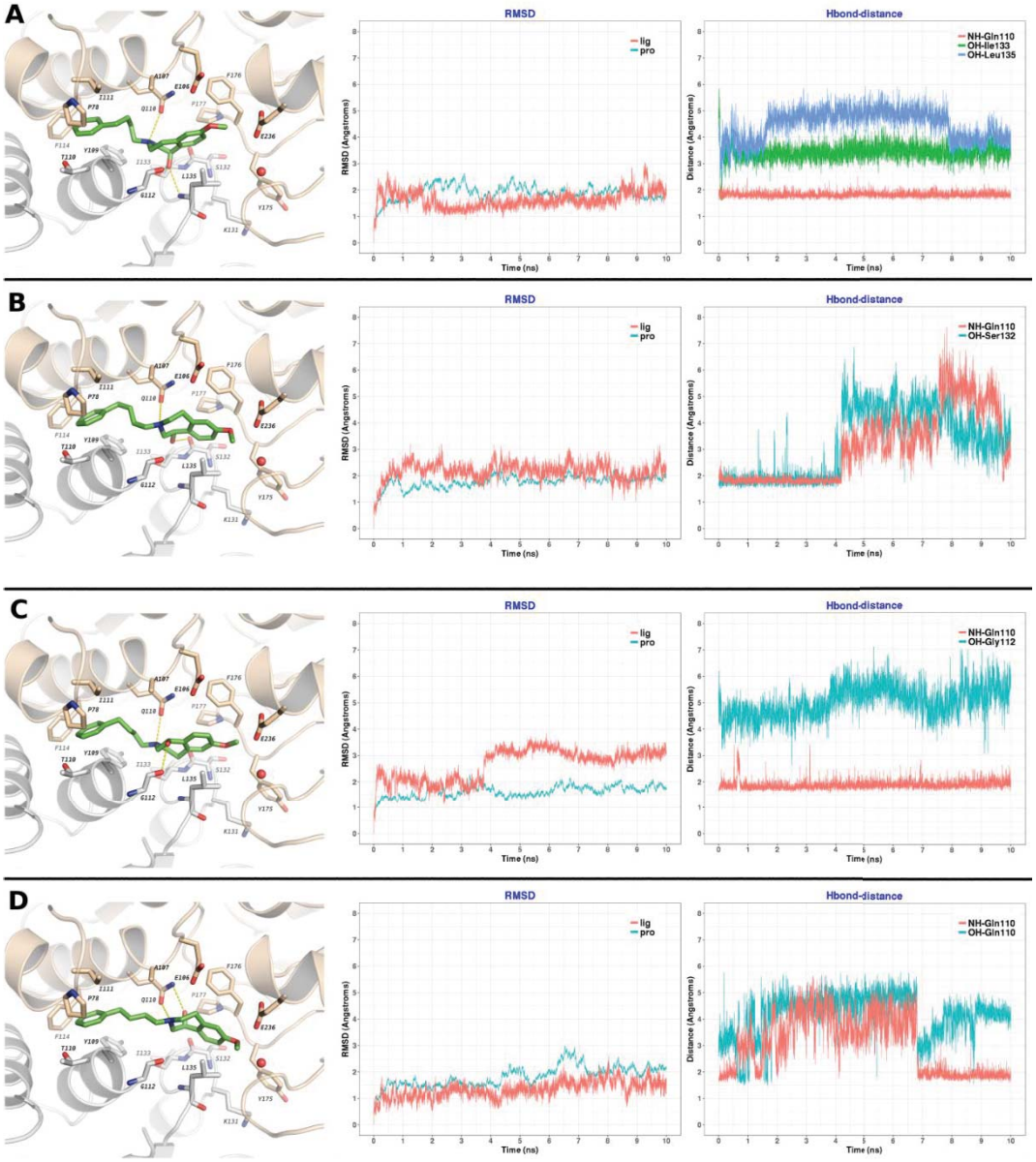

Supplemental Figure 6: Molecular dynamics simulation of the less stable binding modes of ***(R)*-Me-NB1** (**A** and **B**) and ***(S)*-Me-NB1** (**C** and **D**).

Supplemental Table 1: Calculated MM-GBSA binding free energies (kcal/mol) for the two most stable ***(R)-*** and ***(S)*-Me-NB1** binding modes using different GB models. Standard error of the mean (SEM) is given in brackets.

	GB1	**GB2**	**GB5**	**GB8**
***(R)*-Me-NB1**	-59.99 (0.43)	-56.38 (0.44)	-60.56 (0.47)	-51.61 (0.58)
***(S)*-Me-NB1**	-54.90 (0.53)	-49.57 (0.53)	-53.71 (0.56)	-39.04 (0.78)

A

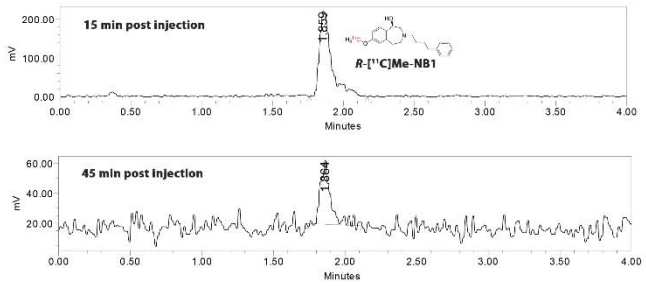

B

Brain

Time (min)	*(R)*- [^{11}C]Me-NB1 (%)	metabolites (%)
0	100	0
15	100	0
45	100	0

Plasma

Time (min)	*(R)*- [^{11}C]Me-NB1 (%)	metabolites (%)
0	100	0
5	79.5	20.5
15	57.5	42.5
45	42.2	57.8

Supplemental Figure 7: Metabolite study with *(R)*-^{11}C-Me-NB1 was performed in male Wistar rats. **A**. Radio-UPLC analysis of the brain samples after 15 and 45 min post injection revealed the presence of parent tracer. No radiometabolite was detected. **B**. Radio-TLC analysis confirmed the radio-UPLC findings for the brain samples. Plasma data at 45 min post injection indicate that 42.0% of the intact parent was still present.

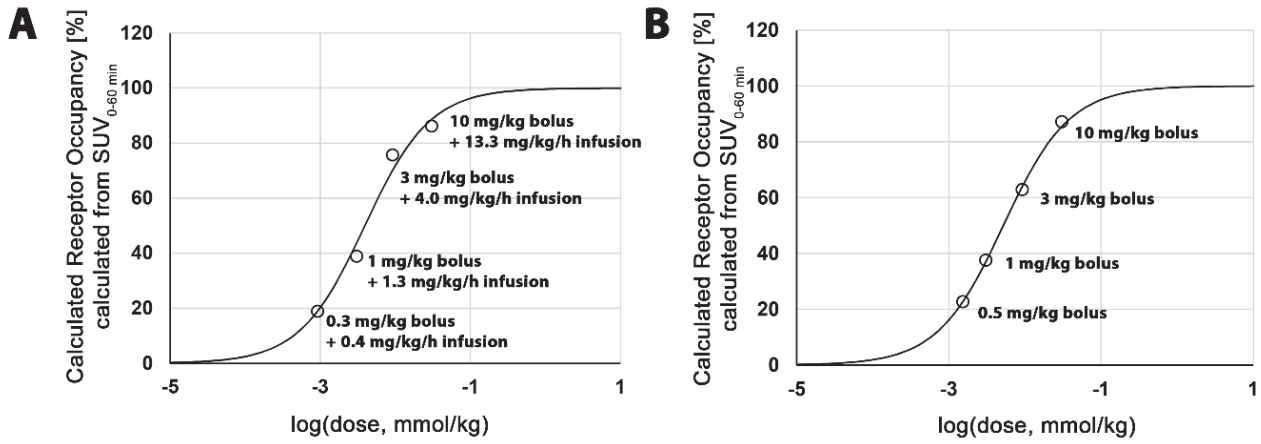

Supplemental Figure 8: Receptor occupancy studies with *(R)*-^{11}C-Me-NB1 and GluN2B-antagonist CP101,606 in male Wistar rats. **A**. Target occupancy was studied upon bolus injections, followed by infusion of CP101,606 to maintain constant plasma levels. **B**. Target occupancy was studied upon bolus injection only, without further infusion of CP101,606. The following equations were used to calculate receptor occupancies: AUC = (bmax - bmin) * D_{50}/(D + D_{50}) + bmin; RO = (bmax - AUC)/(bmax - bmin) * 100, where AUC is the area under the curve of the respective PET scan, D_{50} is the dose required for 50 % receptor occupancy, D is the actual dose, RO is the receptor occupancy in % and bmax as well as bmin are the maximum and minimum binding, respectively.

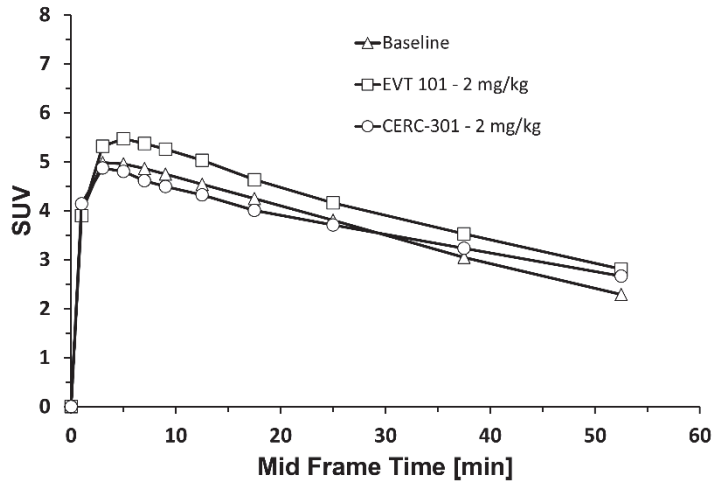

Supplemental Figure 9: PET experiments with *(R)*-^{11}C-Me-NB1 and GluN2B-antagonist CERC-301 and EVT 101 as blocking agents. No blocking effect was observed for the dose of 2 mg/kg, suggesting the lack of *in vivo* target engagement.

Organ	*5 min p.i.*	*15 min p.i.*	*15 min p.i + eliprodil 2 mg/kg*	*30 min p.i.*	*45 min p.i.*	*60 min p.i.*
spleen	0.180 ± 0.014	0.329 ± 0.076	0.290 ± 0.030	0.296 ± 0.030	0.266 ± 0.030	0.196 ± 0.029
liver	0.119 ± 0.015	0.147 ± 0.022	0.146 ± 0.006	0.146 ± 0.013	0.184 ± 0.007	0.176 ± 0.029
kidney	0.588 ± 0.125	0.480 ± 0.019	0.203 ± 0.022	0.378 ± 0.043	0.339 ± 0.041	0.251 ± 0.028
adrenal gland	0.600 ± 0.215	1.597 ± 0.335	0.542 ± 0.045	1.400 ± 0.232	1.344 ± 0.283	1.468 ± 0.395
lung	1.100 ± 0.196	0.479 ± 0.167	0.464 ± 0.061	0.299 ± 0.042	0.220 ± 0.078	0.155 ± 0.028
femur	0.057 ± 0.014	0.068 ± 0.004	0.076 ± 0.010	0.086 ± 0.006	0.083 ± 0.004	0.070 ± 0.014
heart	0.163 ± 0.007	0.086 ± 0.016	0.099 ± 0.008	0.054 ± 0.004	0.050 ± 0.008	0.037 ± 0.003
fat	0.012 ± 0.003	0.035 ± 0.022	0.046 ± 0.009	0.039 ± 0.010	0.048 ± 0.006	0.046 ± 0.009
intestine	0.126 ± 0.008	0.223 ± 0.051	0.305 ± 0.037	0.390 ± 0.069	0.544 ± 0.057	0.521 ± 0.027
testicle	0.041 ± 0.011	0.071 ± 0.017	0.072 ± 0.008	0.092 ± 0.009	0.102 ± 0.011	0.108 ± 0.010
blood	0.022 ± 0.002	0.017 ± 0.002	0.025 ± 0.003	0.015 ± 0.009	0.017 ± 0.000	0.016 ± 0.000
urine	0.043 ± 0.017	0.065 ± 0.022	0.140 ± 0.073	0.141 ± 0.001	0.150 ± 0.053	0.195 ± 0.071
muscle	0.090 ± 0.007	0.074 ± 0.019	0.076 ± 0.006	0.065 ± 0.096	0.057 ± 0.007	0.040 ± 0.004
pancreas	0.487 ± 0.136	0.775 ± 0.170	0.221 ± 0.029	0.766 ± 0.007	0.715 ± 0.055	0.627 ± 0.031
skin	0.030 ± 0.005	0.035 ± 0.007	0.048 ± 0.002	0.054 ± 0.160	0.051 ± 0.005	0.057 ± 0.010
brain	0.353 ± 0.052	0.292 ± 0.040	0.189 ± 0.023	0.256 ± 0.024	0.210 ± 0.018	0.169 ± 0.014

Supplemental Table 2: Organ biodistribution of *(R)*-^{11}C-Me-NB1 in Wistar rats (n=4), reported as averaged % normalized injected dose per gram body weight ± standard deviation. Twenty-four male Wistar rats were tail-vein injected with *(R)*-^{11}C-Me-NB1 (13 – 30 MBq, 0.5 – 4.9 nmol/kg) and sacrificed by decapitation under isoflurane anaesthesia (induced 5 min before decapitation) at the time points 5, 15, 30, 45 and 60 min p.i. (n = 4 for every time point). Additionally, a blockade study was conducted by injection of 2 mg/kg eliprodil in an aqueous vehicle of pH 7.0 containing glucose (5 %), NaCl (0.45 %) and citric acid (1 mM) shortly before the radiotracer and rats have been euthanized at 15 min post injection. The same vehicle was injected into baseline animals shortly before tracer administration. Organs were dissected, weighed and the radioactivity was measured with a gamma-counter. Results were reported as % normalized injected dose per gram organ.

Brain region	*5 min p.i.*	*15 min p.i.*	*15 min p.i + eliprodil 2 mg/kg*	*30 min p.i.*	*45 min p.i.*	*60 min p.i.*
olfactory bulb	0.327 ± 0.039	0.242 ± 0.033	0.149 ± 0.017	0.206 ± 0.018	0.173 ± 0.014	0.135 ± 0.004
hippocampus	0.291 ± 0.053	0.250 ± 0.039	0.192 ± 0.021	0.236 ± 0.019	0.213 ± 0.020	0.174 ± 0.017
thalamus	0.337 ± 0.046	0.304 ± 0.039	0.212 ± 0.024	0.271 ± 0.032	0.221 ± 0.019	0.176 ± 0.016
cerebellum	0.292 ± 0.048	0.248 ± 0.027	0.175 ± 0.025	0.204 ± 0.020	0.158 ± 0.014	0.129 ± 0.011
brain stem	0.275 ± 0.035	0.260 ± 0.038	0.173 ± 0.019	0.266 ± 0.022	0.239 ± 0.018	0.213 ± 0.025
midbrain	0.322 ± 0.045	0.294 ± 0.048	0.187 ± 0.021	0.282 ± 0.026	0.236 ± 0.019	0.195 ± 0.020
cortex	0.430 ± 0.063	0.329 ± 0.048	0.198 ± 0.024	0.273 ± 0.026	0.218 ± 0.018	0.164 ± 0.011
restbrain	0.225 ± 0.035	0.229 ± 0.036	0.177 ± 0.030	0.216 ± 0.016	0.200 ± 0.022	0.183 ± 0.028
striatum	0.360 ± 0.072	0.306 ± 0.053	0.200 ± 0.025	0.253 ± 0.026	0.202 ± 0.011	0.155 ± 0.013

Supplemental Table 3: Regional biodistribution of *(R)*-^{11}C-Me-NB1 in the Wistar rat brain (n=4), reported as averaged % normalized injected dose per gram body weight ± standard deviation.

JNM The Journal of NUCLEAR MEDICINE

Preclinical Evaluation of Benzazepine-Based PET Radioligands *(R)*- and *(S)*-^{11}C-Me-NB1 Reveals Distinct Enantiomeric Binding Patterns and Tightrope Walk between GluN2B- and Sigma1 Receptor-Targeted PET Imaging

Ahmed Haider, Adrienne Müller Herder, Stefanie D Krämer, Jasmine Varisco, Claudia Keller, Katrin Frauenknecht, Yves P. Auberson, Louisa Temme, Dina Robaa, Wolfgang Sippl, Roger Schibli, Bernhard Wünsch, Linjing Mu and Simon M. Ametamey

J Nucl Med.
Published online: January 25, 2019.
Doi: 10.2967/jnumed.118.221051

The Journal of Nuclear Medicine is published monthly.
SNMMI | Society of Nuclear Medicine and Molecular Imaging
1850 Samuel Morse Drive, Reston, VA 20190.
(Print ISSN: 0161-5505, Online ISSN: 2159-662X)

SNMMI SOCIETY OF NUCLEAR MEDICINE AND MOLECULAR IMAGING